POAC'23
Glasgow, UK

Proceedings of the 27th International Conference on
Port and Ocean Engineering under Arctic Conditions
June 12-16, 2023, Glasgow, UK

Numerical study on the movement pattern of ice around the ship in the broken ice field

Kai Zhong[1]; Bao-Yu Ni[1]*; Zhi-Yuan Li[2]; Yan-Zhuo Xue[1]

1 College of Shipbuilding Engineering, Harbin Engineering University, Harbin 150001, China
2 Department of Mechanics and Maritime Sciences, Chalmers University of Technology, Gothenburg, Sweden

Corresponding author Email: nibaoyu@hrbeu.edu.cn

ABSTRACT

Broken ice field is among the common type of ice conditions when ships operate in Arctic navigation, where ships face a significant increase in resistance and local structural safety threats due to the interaction between the ship's hull, water, and broken ice. The hull needs to remove a large amount of broken ice from its path and disturb the surrounding broken ice, and the extent to which can reflect the intensity of the ship-water-ice interaction. In this study, a coupled CFD-DEM approach to simulate ship-water-ice interaction-related phenomena. In the calculation process, rigid particles are considered as non-rebreakable broken ice, while the effect of ship wave variations on the movement of broken ice is taken into account. The "ice boundary layer" (IBL) is found in the numerical results, and distribution of the thickness of "IBL" along the ship's bow is derived and in good agreement with the formula proposed by Aboulazm (1989). After that, the relationship between ship speed on the movement of ice is also studied.

KEY WORDS: Broken ice field; Ship-water-ice interaction; Ice boundary layer; Coupled CFD-DEM approach.

1 INTRODUCTION

With global warming, shipping and research activities in the polar regions are becoming more frequent (Bergström et al., 2020; Li et al. 2020), and it is more common for ships to encounter broken ice fields. Ice-covered waters pose many challenges for ships. When navigating in the broken ice fields, the most significant problems faced by polar ships are the surge in ship resistance and the threat to structural safety from ice loads (Hu and Ma, 2021). Studies of ship-water-ice interactions help to understand these problems. The movement pattern of the broken ice is the cause of these problems, which in turn have a profound influence on the design of polar ships as well as the ancillary navigational equipment (Ni et al. 2022).

In recent years, the numerical method has become a means of ship-ice interaction. One of the most widely used methods is the simulation of sea ice using the DEM method (Hopkins et al. 1999; Long et al. 2018). For the ship-ice interaction process, the DEM has an advantage in terms of its ability to consider simultaneous contacts between numerous elements. However, Huang et al. (2020) found that the ship-ice interaction changes when considering variations in the flow field, with the ship's waves pushing the broken ice away from the ship and

subsequently causing the ice resistance to decrease. Considering the water effect by the DEM method itself is a challenge. In the broken ice field, the fluid variation can be solved by using a coupling method, such as CFD-DEM (computational fluid dynamics and discrete element method), whose effectiveness has been proven. Previous studies (Luo et al.,2020; Zhang et al., 2022) applied the CFD-DEM coupling method to study ship navigates in a broken ice channel, and both the ship resistance as well as the motion of broken ice compare well with the ship model tests. However, the extent of ship-ice interactions during the ship's navigation is less explored, especially for quantifying the disturbance to broken ice.

This paper focuses on a ship navigating through a broken ice field with a high ice concentration (η =70%), a series of CFD-DEM-based numerical simulations are carried out to investigate the ship-water-ice interaction process. According to the velocity variation of broken ice around the ship, the "ice boundary layer" is found in numerical simulation, and the extent of broken ice disturbance is measured to determine the "ice boundary layer" thickness as well as its distribution at various locations on the bow. which is compared with previous analytical studies, and the differences between them are analyzed. Then the effects of different ship speeds are analyzed.

2 NUMERICAL METHODS AND SETUP

The key to the numerical study of the coupling ship-water-broken ice is the accurately simulate of broken ice movements under the combined influence of ship and water. The CFD-DEM coupling method is a kind of Euler-Lagrangian coupling approach. The CFD method based on the Eulerian viewpoint solves the variation of the fluid field, while the discrete element method based on the Lagrangian viewpoint constructs the broken ice and calculates the forces on it and its motions. In addition, the fluid forces on the broken ice and the forces acting on the fluid field by this broken ice are a pair of mutual forces, and the interaction between broken ice and water is transmitted through both in the CFD-DEM method (Norouzi, et al. 2016). In recent years, there has been a growing number of studies of ship-water-ice interactions using CFD-DEM methods, the validity of which has been well-proven (Luo et al. 2020; Ni et al. 2022; Zhang et al. 2022).

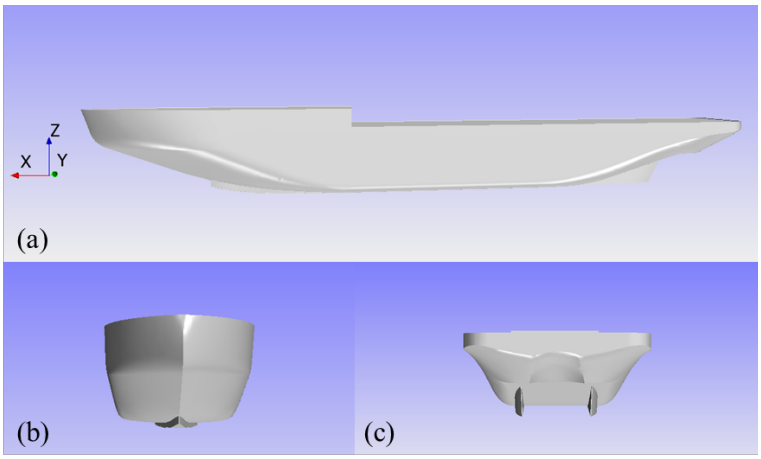

Fig.1 Sketch of the hull model: (a) Side view of the hull; (b) Front view of the bow; (c) Aft view of the stern.

In this paper, the CFD-DEM coupling process was applied in the simulation based on the commercial software Star-CCM+ (Siemens PLM Software, 2019). The hull model used in the

simulation is shown in Figure 1, which is a scaled-down model of an icebreaker with an overall length of 122.5 m, the scale λ is 60.0, and the specific data of the model ship are shown in Table 1.

Table 1. The main parameters of the ship (an ice breaker) model.

Parameter	Unit	Value
Overall length (L)	m	2.04
Molded breath (B)	m	0.37
Draught (T)	m	0.13
Stem angle (γ)	deg	20
Water line angle (α)	deg	34
Flare angle (β)	deg	53

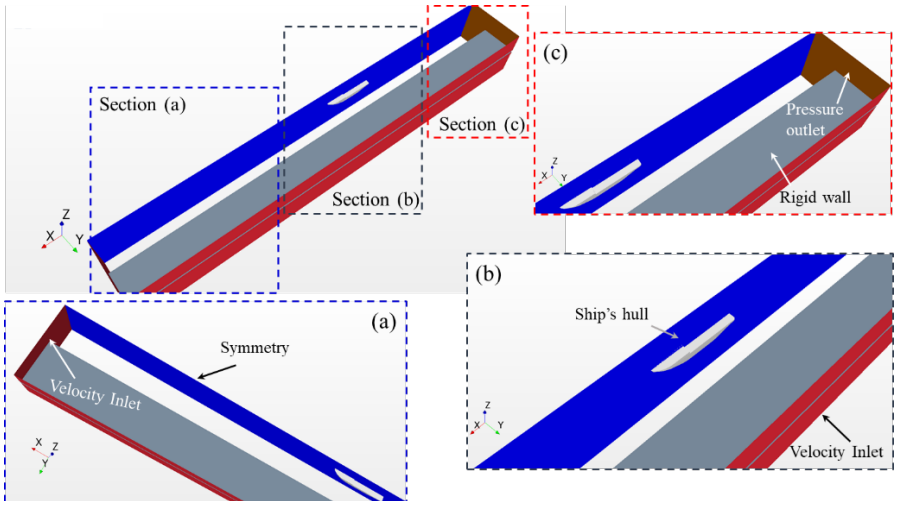

Fig.2 Computational domain and boundary conditions.

In the computational domain setup, the fluid domain is set as 8.65 L in length, 2.40 L in width, and 1.00 L in height. Within the height of 1.0L in the computational domain, the water domain is 0.543L high and the air domain is 0.457L high. The boundary conditions of the computational domain are shown in Figure 2. Where the symmetry of the domain is exploited, the hull is split from the mid-longitudinal section and symmetric boundaries are applied, thus saving computational resources by only calculating for half of the domain. The hull surface is set as a rigid wall, which is also applied at a distance of 1 m from the symmetry boundary to simulate the ice sheet to simulate the broken ice channel.

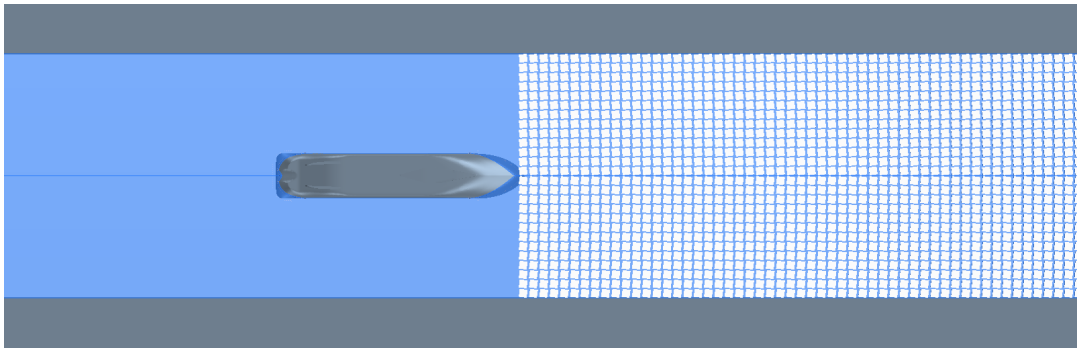

Fig.3 The initial arrangement of the computational domain (η =70%, upward view).

The initialization scene of the calculation domain after the arrangement of broken ice is shown in Figure 3, the broken ice field is arranged in front of the bow and its length is 4.0L. The relative velocity method is adopted in this simulation, which means that the ship model is kept stationary whereas the fluid together with the ice particles exerts a specific velocity astern. In ship-water-ice interactions, the validity of the relative velocity method has been proven (Huang et al. 2020) and it can lead to higher computational efficiency. With regard to broken ice, since this paper is concerned with the interaction between the hull and small pieces of broken ice, which has a side length of 0.067m and a thickness of 0.015m, re-breaking of broken ice is not common at this time. Therefore, the simulation uses non-breakable DEM polygon particles for the broken ice field.

3 RESULTS AND DISCUSSIONS

3.1 Case study on the movement of broken ice

In this section, based on numerical simulations of the ship-water-ice interaction process, a detailed description of the movement of broken ice is made. The ship speed is taken as 0.4 m/s, while the ice concentration is taken as 70%.

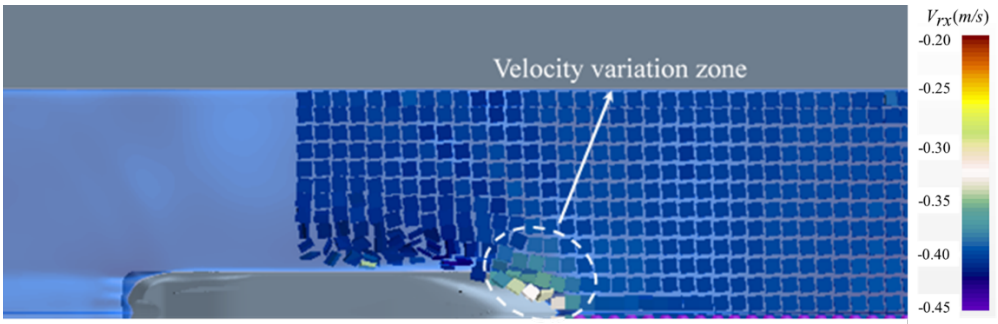

Fig. 4 The contours of the relative velocities of broken ice to ship in the x-axis.

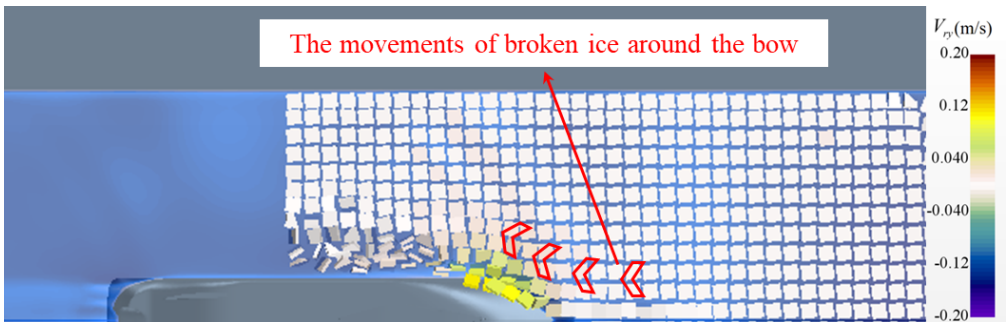

Fig. 5 The contours of the relative velocities of broken ice to ship in the y-axis.

The velocity of broken ice can be easily obtained from numerical simulations. After the ship has fully entered the broken ice field, the relative velocities of broken ice to ship in the y-axis and x-axis V_{ry} and V_{rx} are shown in Fig. 4-5. In Fig. 4, V_{rx} is negative, as its direction is opposite to the x-axis. It can be observed that V_{rx} decreases sharply near the bow area, mainly because of the interaction with the ship bow, as shown by the 'velocity variation zone' in Fig. 4. As the ship moves forward, V_{ry} at both sides of the ship is increased, denoting that the broken ice is pushed outwards (Fig. 5). From Fig. 4-5, especially Fig. 5, one can see that a layer forms around the ship surface, in which the broken ice is significantly affected by the ship and beyond which

the broken ice is only affected marginally. This layer is referred to as the 'ice boundary layer' (Aboulazm, 1989), within which the broken ice is affected by the broken ice directly displaced by the advancing ship.

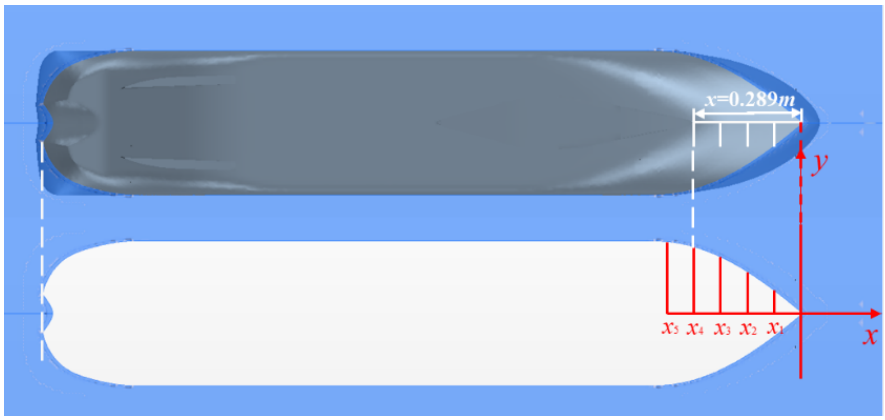

Fig. 6 Ship's hull versus waterline surfaces.

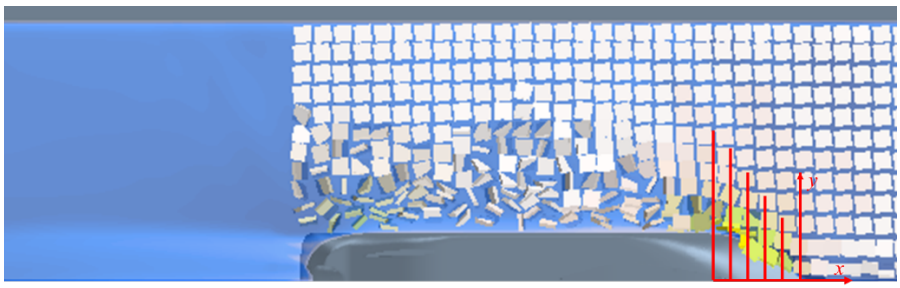

Fig. 7 Furthest distance of disturbed broken ice around the bow.

The "ice boundary layer" can represent the extent of the ship's effect on the broken ice field. It is necessary to identify the furthest distance that the ice is disturbed and the ship's boundary, between which is the thickness of the "IBL" (T). In order to measure the thickness of "IBL" around the bow area, a coordinate system is established with the hull, using the most forward point of the waterline surface as the origin and the forward positive direction of the x-axis. The spatial variation of the "IBL" is investigated by taking five measurement points evenly along the x-axis from the bow to the shoulder of the ship, as shown in Figure 6. The ship's boundary refers to the waterline and the half-waterline widths (Y_w) for the five points selected are measured, the results are shown in Table 2. Afterward, the furthest distance (Y_i) at which the broken ice is disturbed needs to be determined. As shown in Figure 7, the distance of the boundary of compacted broken ice can be determined based on the V_{ry} scenario, the results of which are shown in Table 2. Subsequently, the numerical results of the thickness of the "ice boundary layer" (T_1) are also determined at each location by $T_1 = Y_i - Y_w$, as shown in Table 2.

Table 2 Numerical results of "ice boundary layer" thickness at different locations

Location number along the x -axis	x_1	x_2	x_3	x_4	x_5
Half-waterline width Y_w (m)	0.0627	0.112	0.151	0.176	0.188
Furthest distance of disturbed broken ice Y_i (m)	0.258	0.342	0.444	0.543	0.616

$T_1 = Y_i - Y_w$	0.195	0.230	0.293	0.367	0.428

In addition, the theoretical prediction of the "ice boundary layer" thickness (T_2) for the same conditions can be obtained from the theoretical equation (Eq. 1) proposed by Aboulazm (1989):

$$T_2 = \eta Y_w(x_i)/K_c(1-\eta) \quad (1)$$

Where η is the ice concentration, K_c is the broken ice compacting coefficient, K_c is taken to be 1.0 since the broken ice is square. The comparison of T_2 with the numerical results is shown in Figure 8.

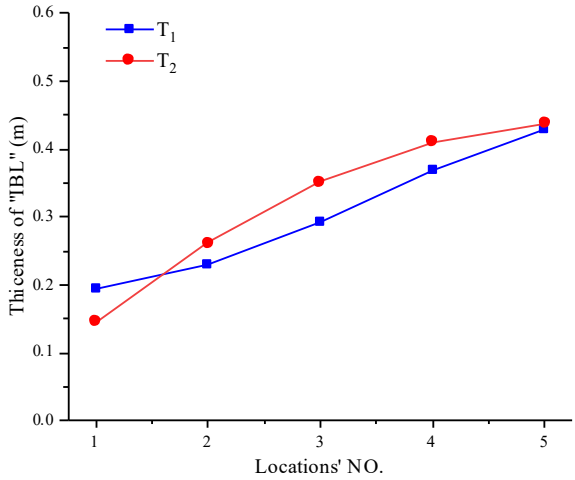

Fig. 8 Comparision of the numerical and theoretical thickness of “IBL”

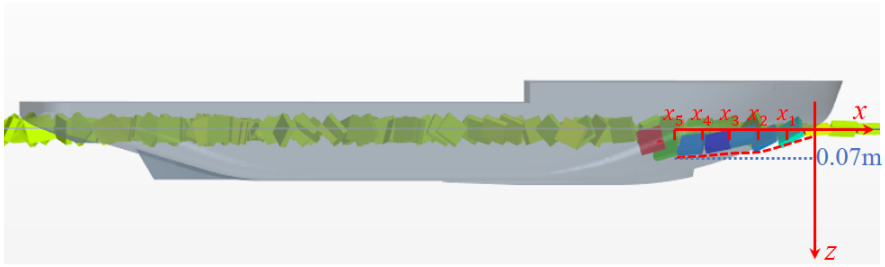

Fig.9 Side view of broken ice around the bow

As shown in Figure 8, T_1 and T_2 have some correspondence, but there are some differences in the spatial distribution trends between them. Firstly, in terms of spatial trends, T_2 represents the theoretical development of the “IBL” in a two-dimensional scenario. Since it cannot take into account the overturning and the sliding of broken ice onto the bottom of the ship, as the waterline moves forward, the broken ice has to be compressed only along the normal direction of the waterline, so the spatial distribution of T_2 trends more similarly to the shape of the waterline expanding outwards. In contrast, T_1 reflects a different trend. Firstly, at x_1, T_1 has a higher estimate of the thickness of “IBL”, which means that the “IBL” formed on the front side of the bow is fuller than theoretically predicted. At these latter points, the value is smaller than T_2. As can be seen in Figure 7, where some broken ice is pushed under the bow at points 2 and 3, and at point 4, where the ice under the ship flips over and reaches the side of the ship. After point 5, the ice come up near the surface and began to exert an influence on the ice field next to the ship. In Figure 9, the scene of overturning broken ice below the waterline can be seen more clearly, with the broken ice mostly clinging to the bottom of the bow and the depth of submersion slowly increasing, and the maximum submersion depth (D_z) is 0.07 m.

3.2 The effect of ship speed

In order to analyze the effect of ship speed on the "ice boundary layer", we carry out simulations at four different speeds: 0.4, 0.5, 0.6 and 0.7 m/s.

(a) V=0.4 m/s

(b) V=0.5 m/s

(c) V=0.6 m/s

(d) V=0.7 m/s

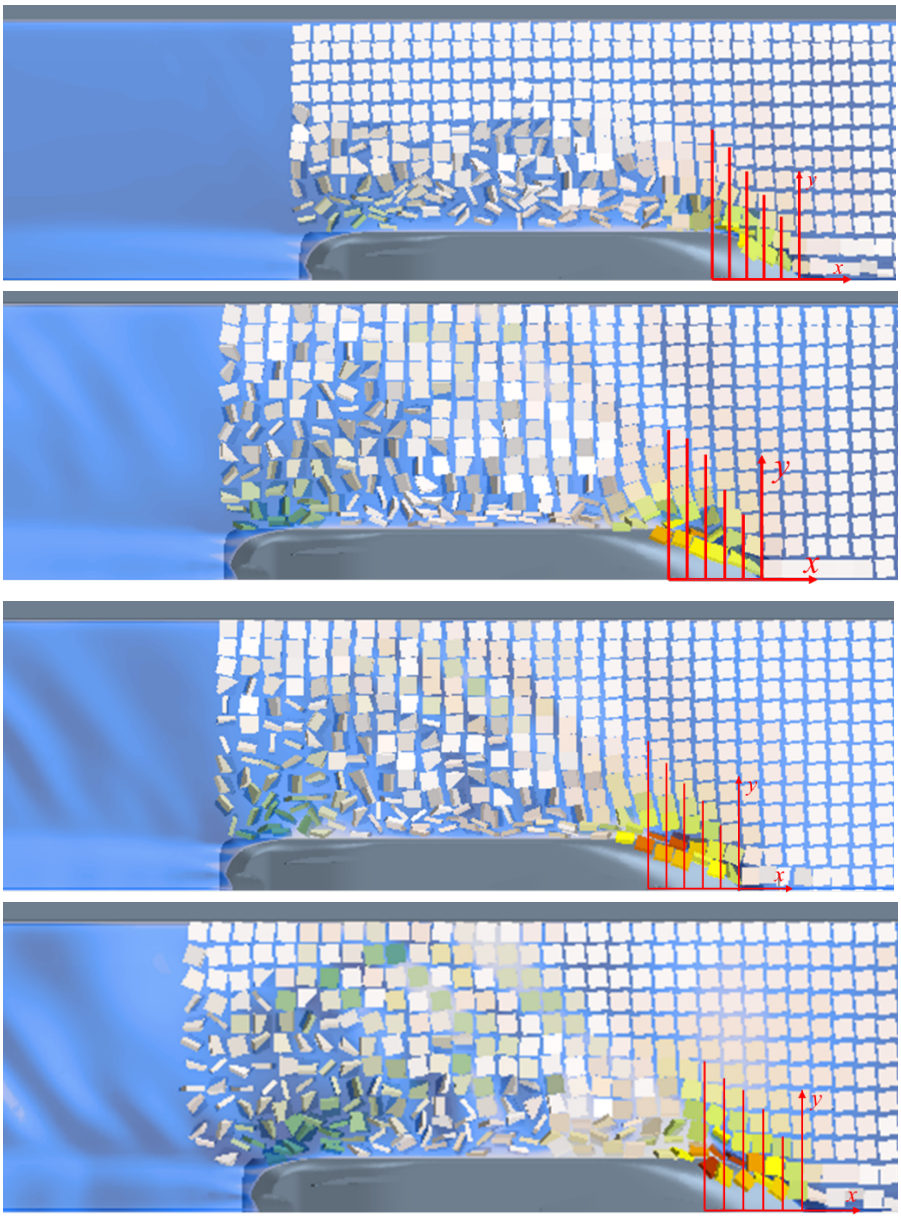

Fig. 10 Simulated scenarios of "IBL" at various ship speeds

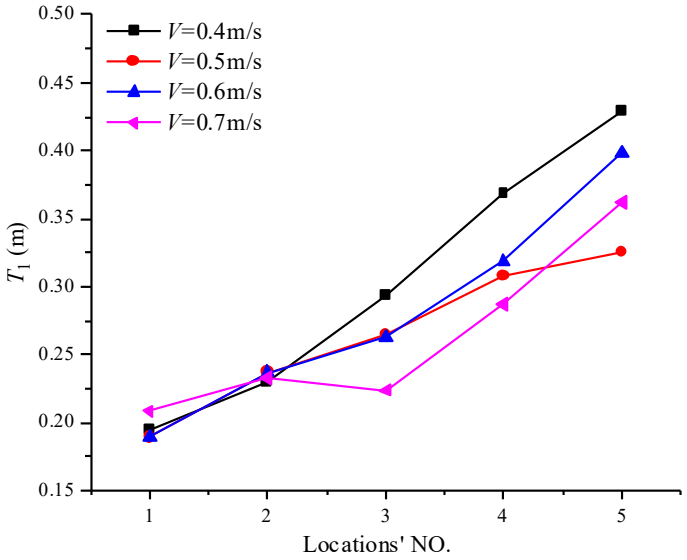

Fig. 11 Numerical thickness of "IBL" at various ship speeds

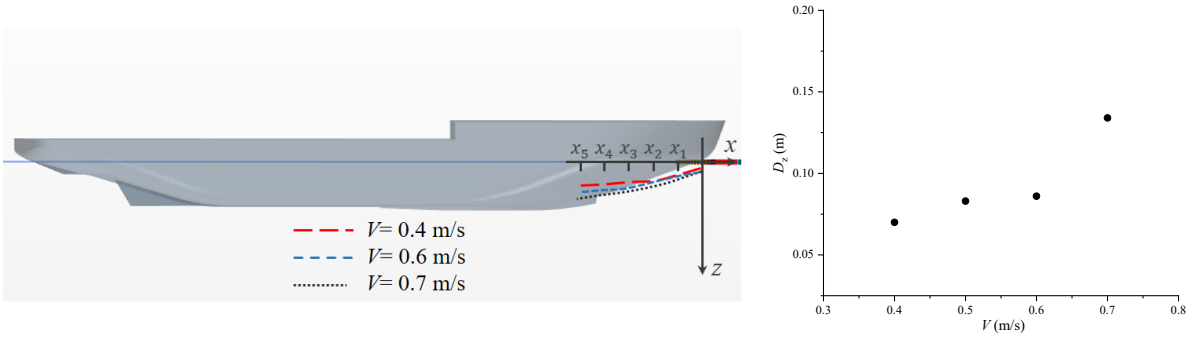

(a) Envelope of submerged broken ice (b) D_z values at different V

Fig. 12 Effect of different speeds on the submergence of broken ice

The simulated scenarios and numerical results of the "IBL" at each ship's speed in the numerical simulation are shown in Figure 10-11. In Figure 11, it can first be seen that at measurement points x_1 and x_2, the thickness of "IBL" is similar at various ship speeds, which means that the increase in ship speed has a small affection on "IBL" in the front of the bow. From measurement point x_3 onwards, the thickness of "IBL" decreases sharply with increasing speed, which means that as the ship speed increases, more of the broken ice is pushed underneath the bow at the last three measurement points, and the area of "IBL" is reduced. This is supported visually by Figure 12 (a), where the dashed line represents the extent of motion of submerged broken ice, and the effect of velocity on the D_z is shown in Figure 12(b). With the envelope gradually moves downwards as the ship speed increases and the degree of ice submergence increases. Correspondingly, more broken ice spends more time on the bottom of the ship and affects the ice field around the ship side later. In addition, the range of the ice submergence is very similar for V=0.5, 0.6m/s, so V=0.5m/s is not shown in this figure.

4 CONCLUSIONS

In this paper, for the movement pattern of broken ice during the ship-water-ice interaction, the formation and thickness of the “IBL” around the ship's bow are investigated using CFD-DEM methods. Two main conclusions are drawn from this study:

1) The ship-ice interaction is analyzed in three dimensions, considering the influence of two factors during ship navigation: the overturning of the broken ice and the sliding along the bottom of the bow, the shape of the "IBL" is different from the previous theoretical prediction, and the overall thickness of the "IBL" is less than the theoretical prediction.
2) In the front side of the bow, the ship’s speed has less influence on the variation of the "IBL", while for the rear part of the bow, increasing the ship’s speed will reduce the local thickness of “IBL”. The ship's influence on the broken ice field will become smaller, and the accumulation of broken ice is significantly weakening.

ACKNOWLEDGEMENTS

This work is supported by the National Natural Science Foundation of China (Nos. 52192693, 52192690, 51979051, 51979056, and U20A20327), to which the authors are most grateful. Computations were partially performed by resources provided by the Swedish National Infrastructure for Computing (SNIC).

REFERENCES

Aboulazm A. F. Ship resistance in ice floe covered waters [D]. Memorial University of Newfoundland (Canada). 1989.

Bergström, M., Leira, B. J. & Kujala, P. Future scenarios for arctic shipping [C]// ASME 2020 39th International Conference on Ocean, Offshore and Arctic Engineering, Online, 2020.

Hopkins M.A., Tuhkuri J. Compression of floating ice fields [J]. Journal of Geophysical Research Oceans, 1999, 104(C7):15815-15825.

Huang L.F., Tuhkuri J., Igrec B., et al. Ship resistance when operating in floating ice floes: a combined CFD&DEM approach [J]. Marine Structures, 2020, 74:102817.

Hu Y.H., Ma M.L. Research on key problems of arctic navigation safety [J]. Journal of Physics: Conference Series, 2021, 1827(2021)012094.

Long X., Ji S., Wang Y. Validation of micro-parameters in discrete element modeling of sea ice failure process [J]. Particulate Science & Technology, 2018:1-10.

Li, Z., Ringsberg, J. W., & Rita, F. A voyage planning tool for ships sailing between Europe and Asia via the Arctic [J]. Ships and Offshore Structures, 2020, 15(S1), S10-S19.

Luo W.Z., Jiang D.P., Wu T.C., et al. Numerical simulation of an ice-strengthened bulk carrier in brash ice channel [J]. Ocean Engineering, 2020, 196, 106830.

Norouzi H.R., Zarghami R., et al. Coupled CFD-DEM modeling [M]. United Kingdom: John Wiley & Sons, Ltd, 2016.

Ni B.Y., Wei H.Y., Li Z.Y., et al. Numerical simulation of an air-bubble system for ice resistance reduction [J]. Journal of Marine Science and Engineering, 2022, 2022, 10(9), 1201.

Siemens PLM Software, 2019. Simcenter STAR-CCM+® Documentation Version 2019.

Zhang J.N., Zhang Y., Shang Y.C., et al. CFD-DEM based full-scale ship-ice interaction research under FSICR ice condition in restricted brash ice channel[J]. Cold Regions Science and Technology, 2022, 194, 103454.